WAVELET FRAMES ON GRAPHS DEFINED BY FMRI FUNCTIONAL CONNECTIVITY

Nora Leonardi[⋆†], *Dimitri Van De Ville*[⋆†]

[⋆]Medical Image Processing Lab, Ecole Polytechnique Fédérale de Lausanne, CH-1015 Lausanne
[†]Department of Radiology and Medical Informatics, University of Geneva, CH-1211 Geneva

ABSTRACT

Multiscale representations such as the wavelet transform are useful for many signal processing tasks. Graphs are flexible models to represent complex networks and a spectral graph wavelet transform (SGWT) has recently been developed as a generalization of conventional wavelet designs.

Here we extend the SGWT to obtain a Parseval frame, which conserves energy in the transformed domain and makes the reconstruction easy. Moreover, we also show how to deal with negative edge weights. We then apply the modified SGWT to brain functional connectivity data from two different conditions. This shows that the transform that is adapted to the condition, more efficiently captures coherent activity between inter-connected brain regions.

The extended SGWT holds promise for the spatial analysis of fMRI data because it captures coherent activity of distinct brain regions that are functionally connected.

***Index Terms*—** Graph wavelet transforms, spectral graph theory, brain imaging, functional MRI

1. INTRODUCTION

The wavelet transform is a powerful tool for signal processing, which allows a multiresolution view and sparse representation of piecewise smooth time series and images. These transforms have been designed for both uniformly and non-uniformly sampled data, but limited attempts have been made for complicated, more irregular domains, such as highly interconnected network structures.

Graphs are mathematical objects that allow representing complex structures and to facilitate their study. Several extensions of the wavelet transform to signals defined on graphs have been proposed [1, 2, 3, 4]. Recently, Hammond *et al.* exploited the Fourier-domain representation of the continuous wavelet transform and referred to spectral graph theory to extend this concept to graphs. In particular, the scaled and translated wavelets are defined in the spectral graph domain, which is the analogue of the Fourier domain for graphs and defined as the eigenspace representation of the graph Laplacian L. L relates to the underlying network topology and decomposing a signal into a set of basis functions built from its eigenspace captures interactions of network topology and signal characteristics. The spectral graph wavelet transform (SGWT) has been successfully applied to nonlocal image denoising [5].

Cortical activity in the human brain shows a complex spatiotemporal evolution, which is shaped by underlying connectivity. Spatial wavelets naturally lend themselves to the exploration of the spatiotemporal structure of such activity because they capture the spatial variance in the data. For example, the 2-D spatial wavelet transform was applied to fMRI data to gain insight into the dynamical structure of stimulus-induced activity in the visual cortex [6]. Multiscale functional connectivities were observed, indicating a hierarchical organization, but were limited to the study of one voxel in each one of two selected slices due to the nature of the wavelet transform employed. Moreover, the human brain's complex network is increasingly modeled using graphs. These models have for example shown that the brain exhibits 'small-worldness', which promotes both functional segregation and integration [7]. Applying the SGWT to fMRI data defined on brain graphs will capitalize on the underlying (non-local) connectivity between different brain areas to capture co-activations, and applying it at multiple time points will yield insight into the dynamical structure of activity.

After a brief introduction on spectral graph wavelets in Sect. 2.1, we extend the SGWT by specifying a wavelet generating kernel similar to the Meyer wavelets' construction in Sect. 2.2. This way, we obtain a Parseval frame, which is beneficial for many practical applications due to the energy preservation property between the original and transformed domain and the same analysis/synthesis basis functions. We also generalized the SGWT to deal with negative edge weights of the graph in Sect. 2.3. Finally, in Sect. 3, we demonstrate the suitability of the modified SGWT for fMRI functional connectivity data from two different conditions (resting, movies).

2. SPECTRAL GRAPH WAVELETS

2.1. From the Fourier To the Graph Spectrum Domain

We give a short overview of the construction of the SGWT and refer to [1] for details and proofs.

This work was supported in part by the Swiss National Science Foundation (grant PP00P2-123438), in part by the Société Académique de Genève and the FOREMANE foundation, and in part by the Center for Biomedical Imaging (CIBM) of the Geneva and Lausanne Universities, EPFL, and the Leenaards and Louis-Jeantet foundations.

2.1.1. Classical 1-D Wavelets

The 1-D continuous wavelet $\psi_{s,a}(x) = \frac{1}{s}\psi(\frac{x-a}{s})$, at scale s and location a, can be defined in the Fourier domain as

$$\psi_{s,a}(x) = \frac{1}{2\pi}\int_{-\infty}^{\infty}\hat{\psi}(s\omega)e^{-i\omega a}e^{i\omega x}d\omega. \quad (1)$$

This highlights that scaling ψ by $1/s$ can be completely transferred to the Fourier domain by scaling $\hat{\psi}$ with s and that the wavelets can be interpreted as scaled bandpass filters. Shifting to the location a corresponds to $e^{-i\omega a}$. Before defining the graph Fourier transform, we will introduce the notations for weighted graphs.

2.1.2. Weighted Graphs

Let $G = (V, E, W)$ be an undirected graph consisting of $|V| = N$ vertices that are connected by the set of edges E, which each have a nonnegative weight W. The N-by-N adjacency matrix A is then given by the non-diagonal entries

$$A_{ij} = \begin{cases} w(i,j), & \text{if } (i,j) \in E, \\ 0, & \text{otherwise.} \end{cases} \quad (2)$$

The diagonal degree matrix D is given by

$$D_{ii} = \sum_j A_{ij}, \quad (3)$$

and the Laplacian matrix L is given by $L = D - A$. L is a symmetric, positive semi-definite matrix and thus has a discrete set of N non-negative eigenvalues λ_ℓ with corresponding real eigenvectors χ_ℓ that form an orthonormal basis; i.e. $L\chi_\ell = \lambda_\ell\chi_\ell$ for all ℓ.

2.1.3. Spectral Graph Wavelets

The Fourier transform represents the signal on complex exponentials $e^{i\omega x}$, which are the eigenfunctions of the 1-D derivative operator D; i.e., $D\left\{e^{i\omega x}\right\} = (i\omega)e^{i\omega x}$. In analogy, the graph spectrum is defined by the eigenvectors χ_l of the graph Laplacian L. This way, the spectral graph wavelet $\psi_{t,n}(m)$, at scale t and vertex n, is defined as

$$\psi_{t,n}(m) = \sum_{l=0}^{N-1} g(t\lambda_\ell)\chi_\ell^*(n)\chi_\ell(m), \quad (4)$$

where g is the wavelet generating function that is defined in the spectral graph domain and behaves as a band-pass filter. It is instructive to compare (1) with (4); i.e., the role of the frequency ω is played by the eigenvalues λ_ℓ and the exponentials $e^{-i\omega a}$ and $e^{i\omega x}$ have been replaced by the eigenvectors $\chi_\ell^*(n)$ and $\chi_\ell(m)$ respectively.

We also need to define the scaling function $\phi_n(m)$ to capture the residual "low-pass" components:

$$\phi_n(m) = \sum_{l=0}^{N-1} h(t\lambda_\ell)\chi_\ell^*(n)\chi_\ell(m) \quad (5)$$

where h is the scaling function generator whose design is uncoupled from the choice of g. An example of exact specification was given in [1]. As in the 1-D setting, the wavelet and scaling function coefficients are given by the inner product of the signal f with the wavelets $\psi_{t,n}$ and the scaling function ϕ_n, respectively:

$$W_f(t,n) = \langle \psi_{t,n}, f \rangle, \quad (6)$$

$$S_f(n) = \langle \phi_n, f \rangle. \quad (7)$$

2.2. Parseval Frame Construction

We design the wavelet generating kernel g and the scaling function h in analogy to the Meyer wavelets, for which g and h are defined in the Fourier domain [8]:

$$g(\lambda) = \begin{cases} \sin(\frac{\pi}{2}\nu(\frac{1}{\lambda_1}|\lambda| - 1) & \text{if } \lambda_1 \le \lambda \le \lambda_2, \\ \cos(\frac{\pi}{2}\nu(\frac{1}{\lambda_2}|\lambda| - 1) & \text{if } \lambda_2 \le \lambda \le \lambda_3, \end{cases} \quad (8)$$

$$h(\lambda) = \begin{cases} 1 & \text{if } \lambda \le \lambda_1, \\ \cos(\frac{\pi}{2}\nu(\frac{1}{\lambda_1}|\lambda| - 1) & \text{if } \lambda_1 \le \lambda \le \lambda_2, \end{cases} \quad (9)$$

where, $\nu(x) = x^4(35 - 84x + 70x^2 - 20x^3)$ and $\lambda_1 = \frac{2}{3}$, $\lambda_2 = 2\lambda_1$, $\lambda_3 = 4\lambda_1$. The J wavelet scales are defined as $t_j = 2^j\lambda_{max}^{-1}$ for $j = 0, ...J-1$.

This set of kernels leads to a Parseval frame (also called a 1-tight frame), which is defined as follows: A family of functions $\{e_k\}$ forms a Parseval frame of a Hilbert space $\mathbf{H}$, if

$$\forall f \in \mathbf{H}, \quad ||f||^2 = \sum_k |\langle f, e_k \rangle|^2. \quad (10)$$

Parseval frames have a simple reconstruction formula where the analysis functions are used at the synthesis side:

$$f = \sum_k \langle f, e_k \rangle e_k \quad (11)$$

2.3. Negative Weights

For many applications, such as the one we consider below, the edge weights can be negative in a meaningful way. The Laplacian matrix L as defined above results in an indefinite matrix for negative weights W. We therefore replaced L with the the signed Laplacian $\bar{L} = \bar{D} - A$, where the diagonal matrix $\bar{D}$ is given by

$$\bar{D}_{ii} = \sum_j |A_{ij}|, \quad (12)$$

This definition ensures that the Laplacian is positive-semidefinite and that all eigenvalues are non-negative [9, 10].

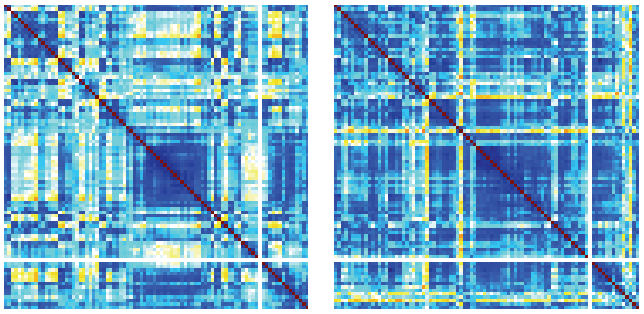

Fig. 1. Signed Laplacian matrices $\bar{L}$ for 90-region functional connectivity graphs during resting (left) and movies condition (right). Warm colors represent positive entries, cold colors negative ones; degree capped at 1 to enhance visibility.

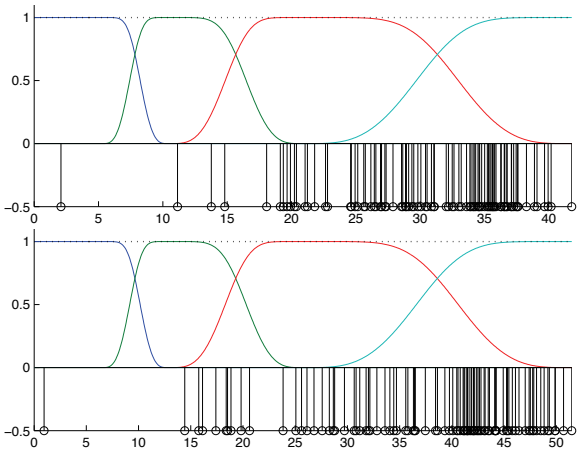

Fig. 2. Scaling function $h(\lambda)$ (blue curve), wavelet kernels $g(t\lambda_\ell)$, frame bound (black dotted line) and eigenvalues of the Laplacian matrices $\bar{L}$ (black spikes) for the resting (top) and movies condition (bottom).

3. RESULTS

3.1. Functional Connectivity Graph

We used fMRI data acquired from one subject during alternating resting and movies conditions on a 3T scanner (TR/TE/FA = 1.1s/27ms/90°, matrix = 64×64, voxel size = 3.75×3.75×4.2mm^3, 21 contiguous transverse slices, 1.05mm gap, 2598 volumes) [11]. After realignment, fMRI data was parcellated into 90 regions according to the Automated Anatomical Labeling (AAL) atlas and regional mean time series were extracted. The time series corresponding to the same condition (rest or movies) were then concatenated and each one decomposed using the discrete wavelet transform. Pair-wise interregional correlations between the wavelet coefficients at the different scales were estimated. The resulting 90×90 correlation matrices can be interpreted as functional connectivity in a specific frequency band [12, 13]. We used both the resting and movies correlation matrices obtained from the low-frequency interval 0.03-0.06Hz (scale 4) for our further analyses. The adjacency matrix A is obtained by setting the diagonal to 0 (i.e., removing loops). Fig. 1 shows the Laplacian matrices $\bar{L}$ for the resting and movies condition, respectively.

3.2. Scaling Function and Wavelet Kernels

The scaling function and wavelet generating kernels for $J = 3$ scales, and the eigenvalues of $\bar{L}$ are shown in Fig. 2. It indicates that, overall, the connectivity is increased during the movies condition (larger eigenvalues than for the resting condition) and that the number of eigenvalues at each scale t_j is comparable between the two conditions.

3.3. Decomposing the FMRI Signal Using the SGWT

For the decomposition, we used the original regional time courses f that alternated between the resting and movies condition, that is, before concatenation. We normalized f at each scan to remove variations in global energy between the two conditions and minimize effects of scanner drifts and movements artifacts (i.e., $||f||^2 = 1$ for each scan). We decomposed f using both the SGWT constructed from the "resting connectivity graph" (resting frame) and the SGWT constructed from the "movies connectivity graph" (movies frame). Fig. 3 shows the sum of the energy of the wavelet coefficients over all brain regions at each scan after applying a moving average of length 2^4, in accordance with temporal scale 4. At the finest scale, we can see that, during the resting conditions, the energy of the wavelet coefficients in the resting frame is smaller than in the movies frame (i.e., blue line below red line) (Table 1). This relation is reversed during the movies block, where the energy of the coefficients in the movies frame is smaller (red line below blue line). At the coarse scale the behavior is reversed: during the resting conditions, the energy of the resting-frame coefficients is lager than that of the movies-frame coefficients (i.e., blue line above red line), whereas during the movies conditions the energy in the movies frame is larger (i.e., red line above blue line). This shows that decomposing the fMRI data using the SGWT adapted to the condition results in fewer large coefficients at the finest scale and more large coefficients at the coarsest scale. The resting frame thus better captures large-scale coherent activity during the resting condition than the movies frame and the inverse is true during the movies condition.

4. CONCLUSION

We constructed graph wavelets and applied them as a new spatial transformation to fMRI data. The graph structure was defined by temporal information; i.e., functional connectivity between the different brain regions. We extended the existing SGWT as a Parseval frame (which provides energy conservation and easy analysis/synthesis) and generalized it to negative edge weights. These extensions allowed applying the

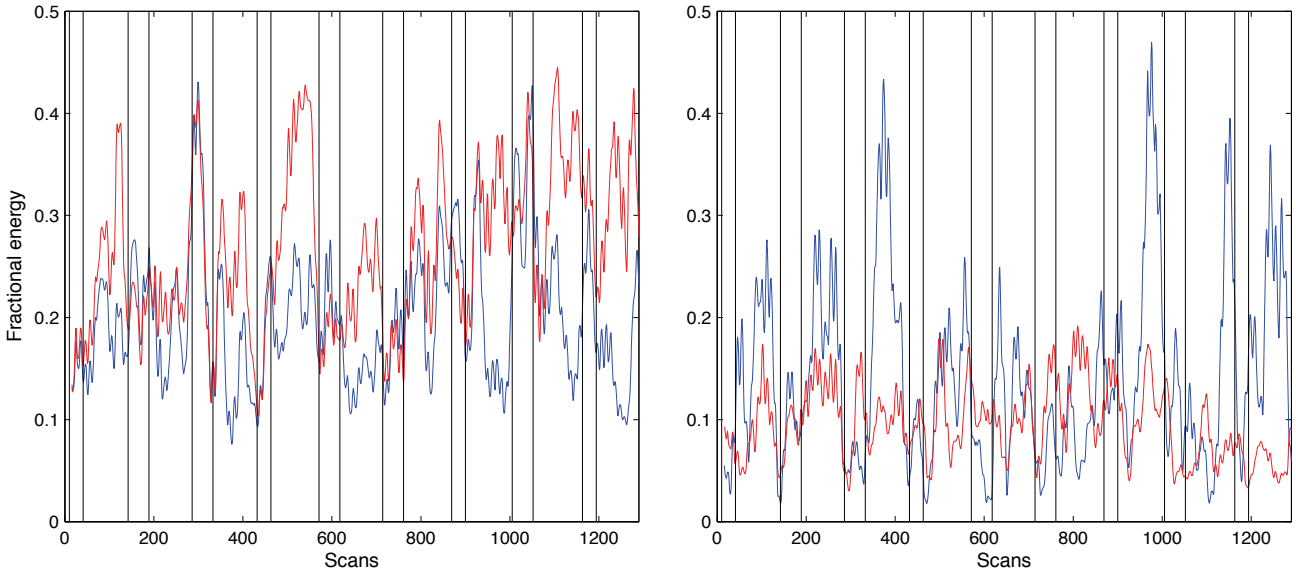

Fig. 3. Sum of the energy of the wavelet coefficients at the finest (left) and coarsest scale (right) over all brain regions, temporally averaged over 2^4 scans. fMRI data was decomposed using the SGWT built from the connectivity graphs of the resting (blue) or the movies condition (red). Vertical bars indicate on- and off-set of the movies condition.

Scale	Condition	
	Rest	Movies
Finest	R	M
Coarsest	M	R

Table 1. Comparison of the energy of the wavelet coefficients at the finest and the coarsest scale for the resting and movies conditions. R indicates that the energy of the coefficients is smaller in the resting than in the movies frame; M indicates that the energy in the movies frame is smaller.

transform to fMRI data and comparing the energy of the coefficients across different scales as a fraction of the energy of the original signal. As a proof of concept, we showed that the decomposition of the fMRI signal using the SGWT matched to the condition was characterized by larger wavelet coefficients at the coarse scale than when using the SGWT adapted to a different condition. The extended SGWT is a promising spatial representation for fMRI data analysis since it represents joint activation/deactivation of multiple brain regions at different scales.

5. ACKNOWLEDGEMENTS

The authors thank Dr. Jonas Richiardi for the help with the fMRI data preprocessing and Hamdi Eryilmaz, Prof. Patrik Vuilleumier and Dr. Sophie Schwartz for providing them with the fMRI data.

6. REFERENCES

[1] D.K. Hammond, P. Vandergheynst, and R. Gribonval, "Wavelets on graphs via spectral graph theory," *Appl Comp Harm Anal*, in press.

[2] R.R. Coifman and M. Maggioni, "Diffusion wavelets," *Appl Comp Harm Anal*, vol. 21, no. 21, pp. 53–94, 2006.

[3] M. Crovella and E. Kolaczyk, "Graph wavelets for spatial traffic analysis," in *Proc IEEE INFOCOM*, 2003.

[4] P. Besson, C. Delmaire, V. Le Thuc, S. Lehericy, F. Pasquier, and X. Leclerc, "Graph wavelet applied to human brain connectivity," in *Biomedical Imaging: From Nano to Macro, 2009. ISBI '09. IEEE International Symposium on*, 2009, pp. 1326–1329.

[5] D.K. Hammond, K. Raoaroor, L. Jacques, and P. Vandergheynst, "Image denoising with nonlocal spectral graph wavelets," in *SIAM Conference on Imaging Science*, 2010.

[6] Michael Breakspear, Ed T Bullmore, Kevin Aquino, Pritha Das, and Leanne M Williams, "The multiscale character of evoked cortical activity.," *Neuroimage*, vol. 30, no. 4, pp. 1230–1242, May 2006.

[7] E. Bullmore and O. Sporns, "Complex brain networks: graph theoretical analysis of structural and functional systems.," *Nat Rev Neurosci*, vol. 10, no. 3, pp. 186–198, Mar 2009.

[8] Y. Meyer, "Principe d'incertitude, bases hilbertiennes et algbres d'oprateurs," *Seminaire Bourbaki*, vol. 662, pp. 209–223, 1986.

[9] Y.P. Hou, "Bounds for the least laplacian eigenvalue of a signed graph," *Acta Math Sin*, vol. 21 (4), no. 21, pp. 955–960, 2005.

[10] J. Kunegis, S. Schmidt, A. Lommatzsch, J. Lerner, E.W. De Luca, and S. Albayrak, "Spectral analysis of signed graphs for clustering, prediction and visualization," in *Proc SDM*, 2010.

[11] H. Eryilmaz, D. Van De Ville, S. Schwartz, and P. Vuilleumier, "Impact of transient emotions on functional connectivity during subsequent resting state: A wavelet correlation approach.," *Neuroimage*, Oct in press.

[12] S. Achard, R. Salvador, B. Whitcher, J. Suckling, and E. Bullmore, "A resilient, low-frequency, small-world human brain functional network with highly connected association cortical hubs.," *J Neurosci*, vol. 26, no. 1, pp. 63–72, Jan 2006.

[13] J. Richiardi, H. Eryilmaz, S. Schwartz, P. Vuilleumier, and D. Van De Ville, "Decoding brain states from fmri connectivity graphs.," *Neuroimage*, Jun in press.